4.1 RECENT PROGRESS IN THE DEVELOPMENT OF DUCTILE-PHASE TOUGHENED TUNGSTEN FOR PLASMA-FACING MATERIALS – C. H. Henager, Jr., R. J. Kurtz, T. J. Roosendaal, B. A. Borlaug, W. Setyawan, and K. B. Wagner (Pacific Northwest National Laboratory), G. R. Odette, K. H. Cunningham, K. Fields, D. Gragg, and F. W. Zok (University of California, Santa Barbara)

OBJECTIVE

The objective of this study is to develop the materials science of fiber-reinforced tungsten composites as candidates for plasma-facing components in future fusion reactors. A dynamic bridging model for W-Cu is introduced and discussed.

SUMMARY

A promising approach to increasing fracture toughness and decreasing the DBTT of a W-alloy is by ductile-phase toughening (DPT) [1-3]. In this method, a ductile phase is included in a brittle matrix to prevent fracture propagation by crack bridging. To examine the prospect of DPT, W-Cu three-point bend samples were deformed at several strain rates and temperatures. Data from these tests are used for the calibration of a dynamic crack-bridging model that can effectively predict elevated temperature crack growth in W-composites. The development and initial testing of a Cu-ligament bridging model based on a micromechanical flow stress model of Cu is discussed. Good agreement with the 3-point bend testing data is demonstrated along with future plans to improve the model.

PROGRESS AND STATUS

Background

Tungsten (W) and W-alloys are the solid materials of choice for the plasma-facing components (PFCs) of future fusion reactors, such as the International Thermonuclear Experimental Reactor (ITER) and Demonstration Power Plant (DEMO), due to their high melting point, strength at high temperatures, high thermal conductivity, low coefficient of thermal expansion, and low sputtering yield [4-8]. However, W and most W-alloys exhibit low fracture toughness and a high ductile-brittle transition temperature (DBTT) that would render them as brittle materials during reactor operations [4, 6, 9]. The DBTT for unirradiated W-alloys typically ranges from 573K to 1273K (300 to 1000˚C) and in a reactor environment radiation hardening would further elevate this range [6, 10, 11]. Metallurgical approaches to toughen W-alloys, including rhenium (Re)-alloying and severe plastic deformation (SPD), have resulted in modest DBTT decreases [10, 12]. However, they would be difficult or impossible to implement, due to high costs and implications to irradiation hardening (Re alloys) or extremely complex processing demands (SPD) [13-15]. To prevent mechanical failure, a toughening mechanism is needed for W before it can be considered effective plasma facing component material (PFCM). W-alloys toughened by engineered reinforcement architectures, such as ductile-phase toughening (DPT), are strong candidates for PFCs. In DPT, a ductile phase is included in a brittle matrix to prevent fracture propagation. This is accomplished by the formation of an intact bridging zone behind the crack tip, which provides reinforcement, resulting in an increase in the remote load stress intensity for continued crack growth with increasing crack length [16, 17]. In Figure 1a, optical evidence of the crack bridging property of DPT can be seen in a W-Cu alloy.

The principles of DPT are illustrated in Figure 1b, which shows a schematic of ductile bridging ligaments stretching across an open crack in a brittle matrix material, such as W [16, 17]. For a brittle material containing a suitable volume fraction of a ductile phase, a highly effective resistance curve toughening mechanism develops as the crack extends. As the crack propagates through a brittle matrix, it leaves a bridging zone of ductile ligaments over a length $\boldsymbol{L}$ behind the crack tip. As the crack extends, $\boldsymbol{L}$ increases. For small scale bridging (SSB), when the bridging zone is much smaller than the length of the crack, $\boldsymbol{L}$ reaches a steady state ($\boldsymbol{L} = \boldsymbol{L_{SSB}}$). The ligaments act in opposition to the applied loading stress intensity factor, $\boldsymbol{K_{Applied}}$. This reduces the crack tip stress intensity factor so that: $\boldsymbol{K_{Tip}} < \boldsymbol{K_{Applied}}$. The crack

opening (u) increases with increasing distance behind the crack-tip until the reinforcement breaks at a critical u*.

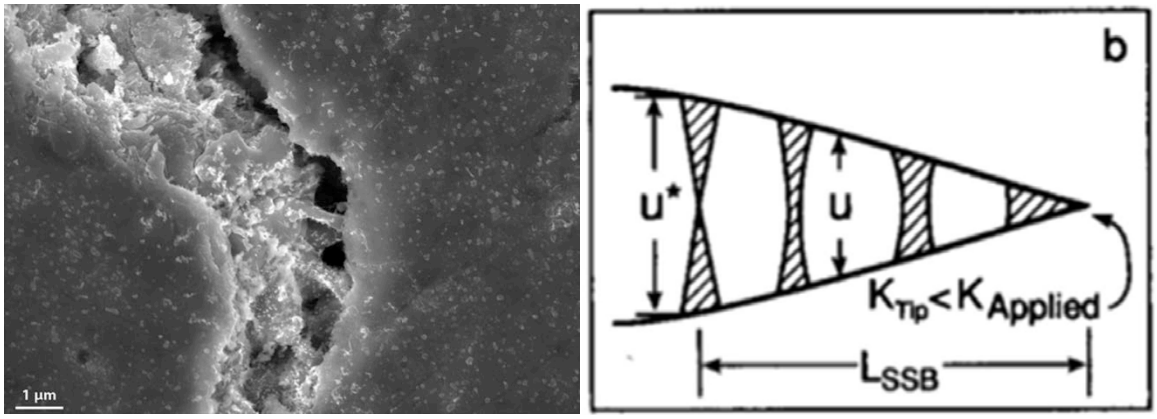

Figure 1. a) SEM image of W-Cu fracture where the ductile phase (Cu) is effectively bridging the crack. b) A steady-state bridging zone shown schematically in 2D [17].

Experimental

Elevated temperature testing of notched and pre-cracked three-point bend specimens was performed in a tube furnace at ½ T_m, ⅔ T_m, and room temperature, where T_m is the melting point of the reinforcement (ductile) phase. Displacement rates of 0.0002, 0.002, 0.02, 0.2, and 2.0 mm/min were employed. Purified Ar gas flowed through the tube furnace to prevent specimen oxidation. W-Cu alloys were evaluated using fracture mechanics test methods to gather quantitative data on the effects of DPT. Similar tests on monolithic W were performed to provide a baseline for comparison to these materials [18].

The W-Cu System

The W-Cu system served as a model system for the initial exploration of DPT in W-alloys [18]. Although not a plausible choice for nuclear applications due to Cu's low melting temperature, it was chosen with the goal of maximizing the plastic $\sigma(u)$ of the Cu reinforcement. The data gathered would be used to develop a fully quantitative model of DPT in the W-Cu system that will aid in future research to develop an effective W-based PFC. A working hypothesis for this composite material is that the fracture properties are determined by the ductile-phase mechanical properties, which in this case is the Cu phase.
The W-25% Cu (by weight) composite, Copelmet®, was purchased by UCSB and sent to PNNL in the form of 3.30mm x 1.67mm x 16.05mm bend bars for mechanical testing [18]. The bars were EDM notched to a depth (a_n) over bar width (w) ratio of a_n/w =0.2. Slight variances in specimen geometry (including notch depth) were accounted for by computing the peak-load linear elastic stress intensity factor (K_{peak}).

Three-Point Bend Testing

Testing was conducted on an Instron 5582 test frame with the following parameters: 1) Test temperatures were ambient, ½ T_m and ⅔ T_m, and 2) Strain rates were 0.0002 to 2 mm/min covering each decade. All high temperature testing was conducted in flowing purified argon (Ar) to prevent oxidation of the sample.

Peak Stress Intensity Calculation

Calculations of K_{Peak} were made from the 3-point SENB data using the peak load and equations A3.1 and A3.2 in ASTM-E399-12, "Standard Test Method for Linear-Elastic Plane-Strain Fracture Toughness KIC of Metallic Materials" [19]. At this stage of research, K_{Peak} provides an approximate toughness-based

method for comparing the mechanical properties of W-composites by accounting for differences in specimen and crack geometry. The results are not meant to be interpreted as fracture toughness data.

Model Development

Model Methodology

A dynamic bridging model was constructed based on previous fiber bridging models with time-dependent deformation, including fiber creep and fiber/matrix interphase oxidation [20-23]. The bridges are now considered to be Cu particles intercepted by cracks in the W matrix. The toughening of the W-Cu alloy has been documented elsewhere [24] but is summarized in Figure 2 showing the dependence of the peak stress intensity, K_{peak}, on 3-point bend sample displacement rate and temperature.
The basic framework of the model is to solve for the set of bridging forces acting on a set of compliant elastic-plastic bridges spanning a crack in a brittle matrix in 2-dimensions (2D) and to treat these forces as crack closure forces that impart a measure of fracture toughness to the brittle matrix material by virtue of having to be deformed plastically as the crack extends. The solution makes use of the weight function for 4-point bending of a bar and is detailed in Ref. [22]. Each Cu bridge is assigned a compliance that is used to compute the bridge force. At this time, we have only implemented the bridge being loaded to its ultimate tensile strength after which it is considered to be a broken bridge and to contribute nothing to crack closure forces.

The model makes use of a published Cu flow stress model [25] to compute the entire flow stress curve to the ultimate strength as a function of strain rate and temperature, which are explicitly built into the flow stress model. In this way, the effects of test strain rate and temperature are accounted for. For the 3-point bend test geometry the experimental displacement rates were converted into an effective tensile strain rate using the 3-point bending formula. These were the strain rates that are used in conjunction with the Cu flow stress model implementation.

Implementation with Cu Flow Stress Model

The flow stress model for Cu as derived in Ref. [25] is implemented. In the model, the stress has an exponential dependence on the strain as follows:

$$\sigma = \sigma_y + \frac{m^2 \alpha G}{\omega c_L}\left(1 - e^{-\omega\varepsilon/2}\right) \tag{1}$$

where σ_y is the yield strength where plastic deformation starts, *m* the Taylor factor, *G* the shear modulus,

$\alpha = (1-\nu/2)/2\pi(1-\nu)$ (ν is the Poisson's ratio), and $\omega = \frac{m}{b} d_{int}\left(2 - \frac{1}{n_{slip}}\right)$. The interaction distance between dislocations where they start to combine, d_{int} is taken to be 2.5 times the Burger's vector magnitude *b*. The number of slip systems n_{slip} in Cu is 12. The parameter c_L is related to the "spurt" distance, *L*, which a dislocation moves when it is released during deformation:

$$c_L = L\sqrt{\rho} \tag{2}$$

where ρ is the dislocation density. The value of c_L is calculated from the stationary dislocation density ρ_{stat}. From the balance of dislocation density due to work hardening and dynamic recovery model:

$$\rho_{stat} = \left(\frac{m}{b c_L \omega}\right)^2 \tag{3}$$

On the other hand, the balance of dislocation density due to work hardening and static recovery model gives

$$M\rho_{stat}^{3/2} = \frac{m\dot{\varepsilon}}{2bc_L}\left(\frac{2}{Gb^2}\right) \tag{4}$$

where *M* is the dislocation mobility, which depends on temperature, *T*, and dislocation density. Using Equation 3 and 4, c_L can be solved numerically. The dislocation mobility for climb and glide is given by

$$M(T,\sigma) = \frac{D_{s0}b}{k_B T}\exp\left(\frac{\sigma b^3}{k_B T}\right)\exp\left(-\frac{Q}{RT}\left[1-\left({}^{\sigma}/_{\sigma_{back}}\right)^2\right]\right) \tag{5}$$

The meaning and value of the constants are given in Table 1. The stress is related to the dislocation density as

$$\sigma = \sigma_y + m\alpha Gb\sqrt{\rho} \tag{6}$$

The dependence of the shear modulus on temperature is taken to be $G = 4.75\text{x}10^4 - 17T$, where *G* is in MPa and *T* in K. The temperature and strain rate dependence of the yield strength is expressed as

$$\sigma_y(T,\dot{\varepsilon}) = \sigma_y(T_0,\dot{\varepsilon_0})\left[\left(1-\left(\frac{\sigma}{\sigma_{back}}\right)^2\right)\left(\frac{\sigma}{\sigma_{CL0}}\right)+\left(\frac{\sigma}{\sigma_{back}}\right)^2\frac{G}{G_0}\right]\left(\frac{\dot{\varepsilon}}{\dot{\varepsilon}_0}\right)^{1/n} \tag{7}$$

where the subscript 0 denotes the reference temperature of 293 K and reference strain rate of 0.0001. The Norton exponent, n, can be determined from the stationary creep rate as follows:

$$\dot{\varepsilon} = \frac{2bc_L}{m}\frac{Gb^2}{2}M(T,\sigma)\left(\frac{\sigma}{\alpha mGb}\right)^3 \tag{8}$$

$$n = d\ln(\dot{\varepsilon})/d\ln(\sigma) \tag{9}$$

This model provides a set of equations that can be solved at a given strain rate or temperature to provide a stress-strain curve, either true strain or engineering strain, that is used to represent the Cu bridges in the dynamic bridging model. At the present time, the bridges are only allowed to reach their ultimate tensile strength and then break. No time-dependent creep deformation is treated at this time, rather the strain rates are accounted for explicitly in the flow stress model. Norton exponents range from 120 at room temperature and fast strain rates to about 6 as slower strain rates and high temperatures. In addition, a strengthening factor, sfact, is introduced into the model to account for bridge size effects and tri-axial constraint. This factor linearly scales the stress strain curve to account for these effects that can act to greatly increase the fracture strength of small, constrained bridges. In this preliminary work, the linear scaling is applied with a constraint that the Young's modulus remains unchanged. Scaling of the Young's modulus will be investigated in the future.

Table 1. Parameters used in the implementation of the copper flow stress model.[1]

Parameter	Value	Description
$\dot{\varepsilon}_0$	0.0001	Reference strain rate
σ_{back}	257 MPa	Maximum back stress
σ_{CL0}	209 MPa	Reference tensile strength
σ_{y0}	74 MPa	Reference yield strength
m	3.06	Taylor factor
α	0.19	Coefficient in Equation 1
D_{s0}	1.31×10^{-5} m^2/s	Coefficient for self diffusion
Q	198000 J/mol	Activation energy for self diffusion
b	2.56×10^{-10} m	Burger's vector magnitude
k_B	1.381×10^{-23} J/K	Boltzmann's constant
R	8.314 J/mol/K	Gas constant

Approach

In an attempt to compare model results to experimental data, an equivalent dataset was considered. The model begins by considering an initial applied K, a_{K0}, for a known specimen geometry and a_0/w, where a_0 is the initial crack length and w is the specimen width. For the case treated here, a_0 was 0.7 mm and w was 3.3 mm and the bar was loaded in 4-point bending. The value of *sfact* was obtained by arbitrarily assuming that a bridged crack that was 1-mm long existed in the sample at each strain rate and temperature. The value of *sfact* that achieved this stable bridged crack at $2/3T_m$ and a strain rate of 1.47×10^{-5} s^{-1} was equal to 4.7. Thus, the computed flow stress for Cu using the flow stress model was scaled by 4.7 to account for size and constraint effects in the Cu bridges. A bridge radius of 50 µm was assumed with a Cu volume fraction of 0.4 to match previous SEM data on Cu area fraction in polished cross-sections.

Results

Model Results

The model was run at all strain rates and temperatures to match the experimental dataset (see Table 2) so that a maximum applied K (a_{K0}) was found for each temperature and strain for which the crack was still bridged and stable after 1-mm of crack growth. The criteria for crack growth was a_{Kcrit} = 8 MPa√m so that a crack will arrest when a_{Ktip} falls below 8 MPa√m. Determining the maximum applied K (a_{Kmax}) for which crack arrest will still occur is roughly equivalent to measuring the K_{peak} in the experiments, and allows for a direct comparison of datasets, one experimental and one model. Several steps were taken in order to determine this value for each strain rate and temperature. In addition to recording a_K, other calculated values were recorded as well: a_{Ktip} and the difference between a_K and a_{Ktip}, which is ΔK. ΔK represents the closure force caused by the bridges, or the toughening due to the bridges. The model dataset is shown in Table 1 and the maximum values of a_K (a_{Kmax}) are plotted as a function of applied displacement rate (strain rate) and temperature in Figure 3 for comparison with Figure 2.

[1] The reference condition corresponds to strain rate of 0.0001 at 293 K.

Table 2. Model results showing computed values of critical parameters for stable bridged cracks

Temp (K)	Displ. Rate (mm/min)	Strain Rate (1/s)	sfact	Max a_{K0} (MPa√m)	Number of bridges	a_{Ktip} (MPa√m)	Max a_K = a_{Kmax} (MPa√m)	ΔK (MPa√m)
293	2	0.17	4.7	19.61	29	7.99	34.82	26.83
293	0.2	0.017	4.7	19.39	30	7.44	35.13	27.69
293	0.02	0.0016	4.7	19.31	30	7.80	34.99	27.19
293	0.002	0.000155	4.7	19.13	30	7.99	34.66	26.67
293	0.0002	1.47E-05	4.7	18.8	30	7.99	34.06	26.08
679	2	0.056	4.7	17.72	31	7.85	32.77	24.92
679	0.2	0.0051	4.7	16.94	31	7.99	31.33	23.34
679	0.02	0.000459	4.7	16.52	32	7.99	31.29	23.30
679	0.002	3.97E-05	4.7	15.47	32	7.99	29.31	21.32
679	0.0002	3.45E-06	4.7	14.75	35	7.99	29.77	21.77
905	2	0.035	4.7	16.25	32	7.99	30.68	22.69
905	0.2	0.0029	4.7	15.04	33	7.99	29.09	21.10
905	0.02	0.00024	4.7	13.88	35	7.99	28.01	20.02
905	0.002	1.87E-05	4.7	12.42	38	7.99	26.86	18.87
905	0.0002	1.37E-06	4.7	10.15	39	7.93	22.45	14.52

Experimental Data for W-Cu

At room temperature, the peak stress intensity of W-Cu (≈20-24 MPa√m) is approximately three times greater than that of monolithic W (≈8 MPa√m) [18]. Figure 2 shows the effects of temperature and deformation rate on the peak stress intensity of W-Cu as determined in experiments in flowing Ar in 3-point bending. As expected the greatest toughening occurs for the highest strain rates and the lowest temperatures, corresponding to where the Cu reinforcement phase is the strongest. The least toughening occurs for the slowest strain rates and higher temperatures.

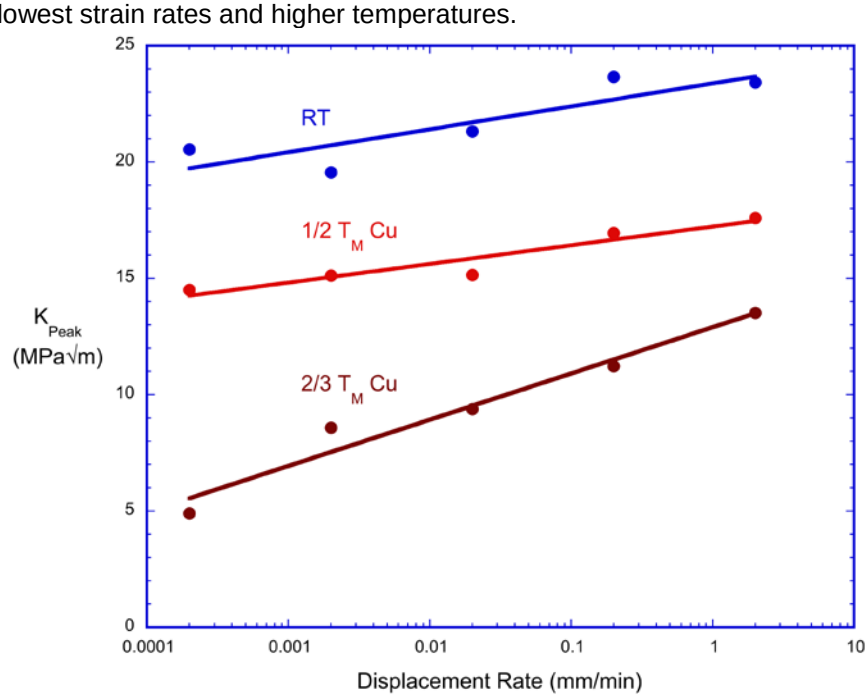

Figure 2. Dependence of peak stress intensity of the W-Cu composite on deformation rate and test temperature.

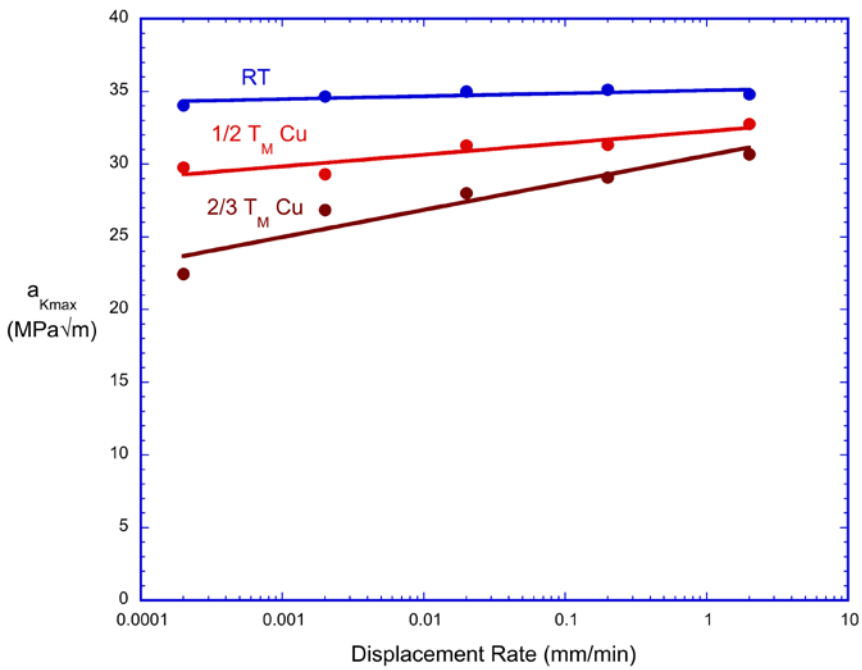

Figure 3. Dependence of computed a_{Kmax} for W-Cu bridged model on strain rate and temperature.

Discussion and Comparison

The model results are rather arbitrary in terms of initial conditions but the trends are encouraging. In order to examine the trends more carefully, the model results are put onto the same scale as the experimental data by applying a simple constant correction. The model a_{Kmax} is scaled to the experimental data by applying a correction of 22.45 – 4.9 = 17.55 MPa√m offset to account for the differences between the model a_{Kmax} and experimental K_{peak} at the slowest strain rate and highest temperature. This scaled result is shown in Figure 4. This data plot demonstrates that the Cu flow stress model captures the effects of strain rate and temperature rather well. The agreement is especially encouraging at the highest temperatures where the slopes of the two datasets as a function of strain rate are very similar. This is attributed to the high quality of the strain rate dependence built to the flow stress model as discussed in Ref. [25]. The two sets of data are not as similar for the room temperature data.

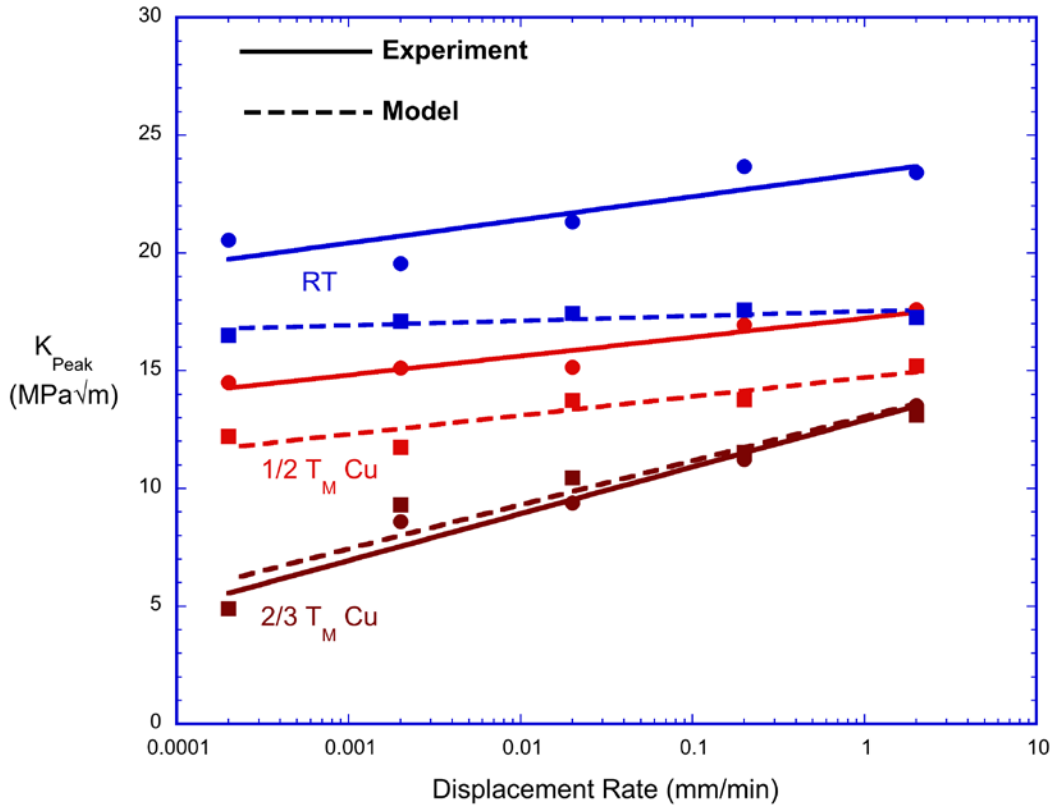

Figure 4. Single point scaled model data compared to experimental data. Solid lines are experiment and dashed lines are model data. The single point scaling places only the two points at the lower left of the plot (slowest strain rate and highest temperature) in coincidence by simple subtraction.
The similarity in slopes at the highest temperatures reflects the accuracy of the Cu flow stress model in capturing the effects of strain rate on ultimate tensile strength. However, it is not clear why this agreement is not as good at room temperature unless the current neglected contributions to bridge deformation (see below) have a larger effect at lower temperatures. Indeed, it may be that we are not capturing the complete work of fracture at room temperature due to the competition between work hardening and plastic instability. At higher temperatures, work hardening is lessened and creep deformation plays an increasingly important role. This work is preliminary and reflects a first-cut at dynamic ductile bridging model development. More details are required.

FUTURE WORK

The representation of the Cu bridges needs to be improved by taking into account the following aspects of ductile bridging as follows:

1. The ductile bridges need to be able to shed load and to neck as seen in experiments [2, 26-28].
2. The ductile bridges need to undergo creep deformation at high temperatures and slow strain rates.
3. The ductile bridges need to be able to debond as required.

REFERENCES

[1] H. E. Deve, A. G. Evans, G. R. Odette, R. Mehrabian, M. L. Emiliani, and R. J. Hecht, Acta Metall. Mater. 38 (1990) 1491.
[2] F. Erdogan and P. F. Joseph, J. Am. Ceram. Soc. 72 (1989) 262.

[3] L. S. Sigl, P. A. Mataga, B. J. Dalgleish, R. M. McMeeking, and A. G. Evans, Acta Metall. 36 (1988) 945.
[4] M. Rieth, J. L. Boutard, S. L. Dudarev, T. Ahlgren, S. Antusch, N. Baluc, M. F. Barthe, C. S. Becquart, L. Ciupinski, J. B. Correia, C. Domain, J. Fikar, E. Fortuna, C. C. Fu, E. Gaganidze, T. L. Galan, C. Garcia-Rosales, B. Gludovatz, H. Greuner, K. Heinola, N. Holstein, N. Juslin, F. Koch, W. Krauss, K. J. Kurzydlowski, J. Linke, C. Linsmeier, N. Luzginova, H. Maier, M. S. Martinez, J. M. Missiaen, M. Muhammed, A. Munoz, M. Muzyk, K. Nordlund, D. Nguyen-Manh, P. Norajitra, J. Opschoor, G. Pintsuk, R. Pippan, G. Ritz, L. Romaner, D. Rupp, R. Schaublin, J. Schlosser, I. Uytdenhouwen, J. G. Van Der Laan, L. Veleva, L. Ventelon, S. Wahlberg, F. Willaime, S. Wurster, and M. A. Yar, J. Nucl. Mater. 417 (2011) 463.
[5] R. A. Pitts, A. Kukushkin, A. Loarte, A. Martin, M. Merola, C. E. Kessel, V. Komarov, and M. Shimada, Phys. Scripta T (2009) 014001.
[6] P. Mertens, T. Hirai, M. Knaup, O. Neubauer, V. Philipps, J. Rapp, V. Riccardo, S. Sadakov, B. Schweer, A. Terra, I. Uytdenhouwen, and U. Samm, Fusion Eng. Des. 84 (2009) 1289.
[7] A. Gervash, R. Giniyatulin, T. Ihli, W. Krauss, A. Makhankov, I. Mazul, P. Norajitra, and N. Yablokov, J. Nucl. Mater. 367-370 B (2007) 1472.
[8] M. Merola, W. Danner, and M. Pick, Fusion Eng. Des. 75-79 (2005) 325.
[9] P. Mertens, V. Philipps, G. Pintsuk, V. Riccardo, U. Samm, V. Thompson, and I. Uytdenhouwen, Phys. Scripta T (2009) 014032.
[10] B. Gludovatz, S. Wurster, A. Hoffmann, and R. Pippan, Int. Journal of Refractory Metals and Hard Materials 28 (2010) 674.
[11] S. J. Zinkle and N. M. Ghoniem, Fusion Eng. Des. 51-52 (2000) 55.
[12] M. Faleschini, H. Kreuzer, D. Kiener, and R. Pippan, J. Nucl. Mater. 367-370 A (2007) 800.
[13] T. Tanno, A. Hasegawa, J. C. He, M. Fujiwara, M. Satou, S. Nogami, K. Abe, and T. Shishido, J. Nucl. Mater., 386-388 (2009) 218.
[14] T. Tanno, A. Hasegawa, M. Fujiwara, H. Jian-Chao, S. Nogami, M. Satou, T. Shishido, and K. Abe, Mater. Trans. 49 (2008) 2259.
[15] T. Tanno, A. Hasegawa, H. Jian-Chao, M. Fujiwara, S. Nogami, M. Satou, T. Shishido, and K. Abe, Mater. Trans. 48 (2007) 2399.
[16] K. T. Venkateswara Rao, G. R. Odette, and R. O. Ritchie, Acta Metall. Mater. 42 (1994) 893.
[17] G. R. Odette, B. L. Chao, J. W. Sheckherd, and G. E. Lucas, Acta Metall. Mater. 40 (1992) 2381.
[18] K. H. Cunningham, K. Fields, D. Gragg, F. W. Zok, J. C. H. Henager, R. J. Kurtz, and T. Roosendaal, Fusion Materials Semiannual Progress Report for Period Ending June 30, 2013, DOE/ER-0313/54, U. S. Department of Energy, 95.
[19] Author, Standard Test Method for Linear-Elastic Plane-Strain Fracture Toughness KIC of Metallic Materials, E399-12 (ASTM International, West Conshohocken, PA, 2012).
[20] C. H. Henager Jr., J. Nucl. Mater., 367-370 (2007) 742.
[21] R. H. Jones and C. H. Henager Jr, J. Eur. Ceram. Soc. 25 (2005) 1717.
[22] C. H. Henager Jr. and R. G. Hoagland, Acta Mater. 49 (2001) 3739.
[23] C. H. Henager Jr., R. H. Jones, C. F. Windisch, Jr., M. M. Stackpoole, and R. Bordia, Metall. Mater. Trans. 27A (1996) 839.
[24] C. H. Henager Jr., R. J. Kurtz, T. J. Roosendaal, B. A. Borlaug, G. R. Odette, K. H. Cunningham, K. Fields, D. Gragg, and F. W. Zok, Fusion Materials Semiannual Progress Report for Period Ending December 31, 2013, DOE/ER-0313/55, U. S. Department of Energy, 23.
[25] R. Sandstrom and J. Hallgren, J. Nucl. Mater. 422 (2012) 51.
[26] M. Bannister, H. Shercliff, G. Bao, F. Zok, and M. F. Ashby, Acta Metall. Mater. 40 (1992) 1531.
[27] B. N. Cox, Acta Metall. Mater. 39 (1991) 1189.
[28] M. F. Ashby, F. J. Blunt, and M. Bannister, Acta Metall. 37 (1989) 1847.